Bulletin of the Seismological Society of America, Vol. 94, No. 2, pp. 650–664, April 2004

Directional Variations in Travel-Time Residuals of Teleseismic *P* Waves in the Crust and Mantle beneath Northern Tien Shan

by V. G. Martynov, F. L. Vernon, D. L. Kilb, and S. W. Roecker

Abstract We study the directional variation in travel-time residuals using 13,820 *P*-wave arrivals from 1,998 teleseismic events ($15° \leq \Delta \leq 98°$, $4.1 \leq m_b \leq 7.3$) recorded in 1991–1997 by the Kyrgyz Digital Seismic Network (KNET). Based on a modified version of the iasp91 model that accounts for the Kyrgyz crustal thickness beneath KNET, we convert *P*-wave travel times to travel-time residuals δt. The dependence of δt on backazimuth is modeled as one-, two-, and four-lobed variations in a horizontal plane (Backus, 1965).

A least-squares fit of the azimuthal variation of δt indicates that the crust in the northern Tien Shan is about 11–15 km thicker than it is in the Kazakh Shield and the Chu Depression. From nine KNET stations, the one-lobe model estimates that the slowest *P*-wave travel-time direction is $-5.0° \pm 4.8°$ (almost directly north) and the magnitude of variation is 1.71 ± 0.13 sec. This result is consistent with an upwelling lower mantle plume. For the two-lobe model, the slowest *P*-wave travel-time directions (anisotropy term) are 89.7° and $269.7° \pm 4.7°$ (i.e., trending east–west). We find *P*-wave velocity anisotropy of 2.0%–2.9% associated with a layer with a thickness of 440 km at the top of the lower mantle. The fast direction of the *P*-wave travel-time (north–south) azimuthal anisotropy at the top of the lower mantle is (1) parallel to the absolute motion of the India plate and (2) close to the direction of the upwelling hot mantle flow. The last result suggests that the azimuthal anisotropy of the travel-time residuals is due to the shape-preferred orientation of middle-mantle material that results from plume intrusion. Shear-wave splitting studies (Makeyeva *et al.*, 1992; Wolfe and Vernon, 1998) estimated the fast polarization direction to be parallel to the strike of the geological structures of the northern Tien Shan ($71° \pm 29°$). Thus, the fast polarization direction determined from these shear-wave splitting studies using KNET data contradicts (differs by >90°) the fast travel-time direction ($-0.3°$ and $179.7° \pm 4.7°$) we determine here using *P*-wave travel-time residuals using KNET data. This suggests that the azimuthal anisotropy determined from *P*-wave travel-time variations and from shear-wave splitting in *SKS* and *SKKS* have different sources.

Introduction

A key for understanding the deformation mechanism of the mantle beneath continents is determined by the relationship of seismic anisotropy to the direction of assumed mantle flow. For the northern Tien Shan, seismic anisotropy is determined mostly from shear-wave splitting (Makeyeva *et al.*, 1992; Helffrich *et al.*, 1994; Wolfe and Vernon, 1998). Shear-wave splitting methods cannot determine the thickness of the anisotropy layer, and therefore the anisotropy solution is constrained from results on the fast polarization direction and seismic phase arrival time delays with respect to the top ~200 km of upper mantle (Silver, 1996; Savage, 1999). For the Tien Shan, shear-wave splitting results show that the fast polarization direction (Wolfe and Vernon, 1998) parallels the trend of the mountain belt, ~east–west, and delay times between the fast and slow (north–south) direction vary from 0.4 to 1.4 sec.

Anisotropy can also be determined from the direction dependence of the seismic-wave travel time; however, this is not often done because in most cases it is difficult to get a good azimuthal distribution of earthquakes. The travel-time residual of the *P* wave δt from teleseismic earthquakes can be used to infer the azimuthal anisotropy of the velocity structure beneath the seismic sensors (Dziewonski and Anderson, 1983; Babuska *et al.*, 1993; Bokelmann, 2002). On

the other hand, for many tectonically active regions, it was recognized that a discrepancy exists between azimuthal variations of teleseismic *P*-wave travel times and *SKS* wave-splitting results obtained for the subcontinental mantle. In central Europe, the fast *SKS* directions are close to the trend of the Hercynian fold belt (Bormann *et al.*, 1993), whereas the fast direction of the *P* wave is primarily normal to that tectonic feature (Dziewonski and Anderson, 1983). A similar discrepancy results from teleseismic data recorded in California; at seismic station Landers (LAC), the shear-wave splitting data net an azimuth of $-54°$ (Silver and Chan, 1991; Savage and Silver, 1993) and *P*-wave data net a direction of northeast–southwest (Dziewonski and Anderson, 1983). These results differ by ~100°, which is much larger than the expected uncertainties.

Based on attenuation results from *S* coda waves in the northern Tien Shan, Martynov *et al.* (1999) showed that the magnitude of seismic backscattering varies with source-receiver azimuth, with minimum values of the quality factor Q_c (*S* coda waves) in the ~east–west direction (Az = 118°) and anisotropy of 4.8 ± 0.8%. The interpretation is that the preferred orientation of the impedance (ρV_s) perturbation in the lower crust and most upper mantle is a fracture-related anisotropy and not related to mantle flow.

In this article, we examine ~2000 earthquakes and study the azimuthal variation of travel-time residuals. We calculate the travel-time residual (δt) by taking the difference between the observed *P*-wave arrival time and theoretically predicted *P*-wave arrival times computed with a 2D velocity model. We also use station anomalies and azimuthal effects to determine lateral variations in the mantle and crustal velocity structure. Our anisotropy results contradict previous results based on shear-wave splitting. We attempt to determine the source of this discrepancy.

KNET Data Analysis and Computational Procedures

The Kyrgyz Digital Seismic Network (KNET) is located in central Asia along the boundary between the northern Tien Shan Mountains and the Kazakh Shield (Fig. 1). The Tien Shan intracontinental orogenic mountain building can be explained by crustal shortening resulting from the India–Eurasia collision, which is about 2000 km south of KNET (Tapponnier and Molnar, 1979; Zonenshain *et al.*, 1990). The Tien Shan is an actively deforming area. The predicted direction of absolute plate motion from the model AM1-2 (Minster and Jordan, 1978) is ~north for middle Asia (Silver and Chan, 1991). The present-day crustal shorting from Global Positioning System measurements is ~20 mm yr^{-1} (Hager *et al.*, 1991; Abdrakhmatov *et al.*, 1996; Zubovich *et al.*, 2001). This region has a high rate of seismicity, and several large earthquakes have occurred in the region (Kondorskaya and Shebalin, 1982), such as the M_s 7.3 earthquake on 19 August 1992 (Mellors *et al.*, 1997). Focal mechanism studies show there is predominately north–south shorting that is accommodated by thrust earthquakes (Junga, 1990).

We examine 1,998 teleseismic ($15° \le \Delta \le 98°$) earthquakes (Fig. 1) recorded between October 1991 and September 1997 by KNET (Vernon, 1992) that are stored in the Preliminary Determination of Epicenter (PDE) catalog. These earthquakes have m_b magnitudes that range between 4.1 and 7.3, and in total we have 14,479 analyst-picked (each by V.G.M.) times of high-precision *P*-wave arrivals. Throughout our 6-yr study period, 12 KNET three-component STS-2 seismic sensors were in operation (Fig. 1).

We calculate travel-time residuals using the origin time and location from the PDE catalog and the 2D iasp91 velocity model (Kennett and Engdahl, 1991) that we have corrected by time δt_c for the Kyrgyz crustal structure beneath KNET:

$$\delta t_a = t_a - (t_{iasp91} + \delta t_c), \quad (1)$$

where t_a and t_{iasp91} are observed and calculated arrival times, respectively. These crustal time corrections are based on a 3D velocity model inferred from KNET data (Ghose *et al.*, 1998). As in previous research (Sabitova, 1989; Roecker *et al.*, 1993), this model marks two main velocity structures beneath KNET: the Kazakh Shield and the Chu Depression (near seismic stations USP, CHM, TKM, and TKM2) and the Kyrgyz Ridge in the northern Tien Shan (near seismic stations AML, UCH, KZA, ULH, EKS2, BGK2, AAK, and KBK). The upper 7 km of the Chu Depression is filled with sediments and has relatively low velocity compared to the consolidated rocks of the Kyrgyz Ridge. But for underlying crust at depths of 7–38 km, the velocity difference is reversed (Table 1).

The iasp91 model predicts the travel time for stations at an elevation (h_e) of 0.0 km. For KNET, the topography is significant and varies above sea level by 0.655 km (CHM) to 3.850 km (UCH). To account for these deviations, we make elevation corrections based on an estimation of velocity V_{Pe} in the upper crust for both geological areas, the Chu Depression and the Kyrgyz Ridge. The travel time through crustal material above sea level

$$\delta t_e = \delta t_{a(st)} - \delta t_{a(chm)} \quad (2)$$

on the path

$$\delta l_e = [h_{e(st)} - h_{e(chm)}]/\cos(i), \quad (3)$$

could be described as a travel-time curve with a slope $p = 1/V_{Pe}$, where "chm" and "st" indicate δt_a and h_e at reference station CHM and any KNET station, respectively, and i is the angle of incidence at the surface.

We determine an arithmetic mean value of δt_e for every station assuming the azimuthal dependence of δt_e because of the Moho depth variation beneath the receiver. To reduce biases due to a nonuniform distribution of earthquakes (Fig. 1), this arithmetic mean is computed from the average values determined in each azimuthal quadrant:

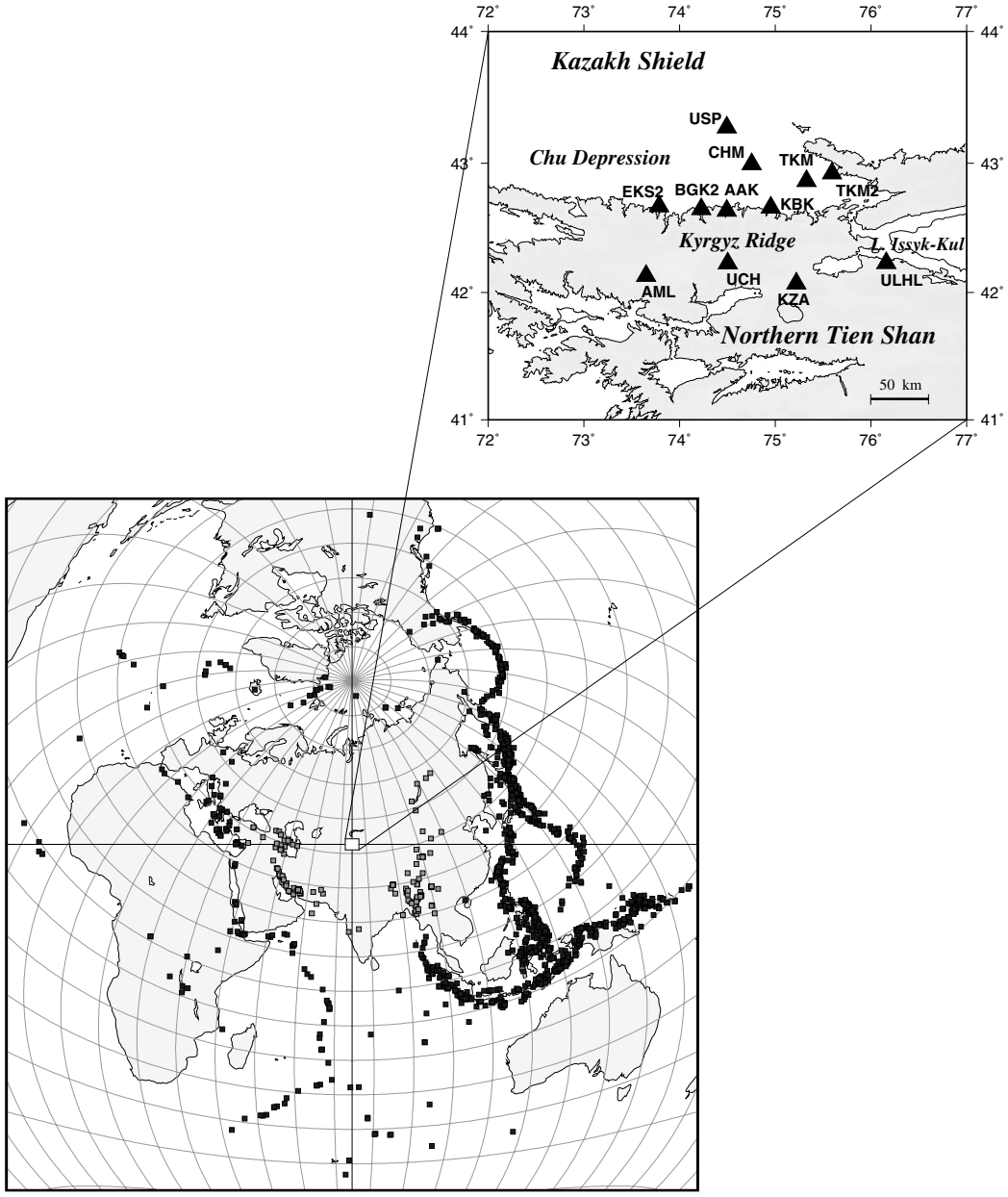

Figure 1. Maps of KNET stations and earthquakes used in this study. Lower map shows the locations of the 1,998 events ($15° \leq \Delta \leq 98°$) recorded between October 1991 and September 1997 (squares). The light and dark gray squares indicate events with distances less than and greater than 31°, respectively. These data are available through the PDE catalog. Only data with $\Delta \geq 31°$ were used to study the azimuthal variations of *P*-wave travel times. This map is drawn using an equal distance projection. Upper map: the station locations for KNET. Shaded area represents elevations above 2000 m.

$$\overline{\delta t}_e = \sum_{k=1}^{4} [\sum_{m=1}^{M_k} (\delta t_e)_{k,m}/M_k]/4, \quad (4)$$

where k is the number of the azimuthal quadrant and M_k is the maximum number of measurements in the kth quadrant.

We initially assume the elevation medium V_{Pe} represented the velocity of the upper crust in our two study regions V_{Po}, 4.90 and 5.50 km/sec (Table 1). Our first estimate ($j = 1$) was reached for (1) V_{Pe} using an regression analysis procedure of $\overline{\delta t}_e$ on δl_e (Fig. 2) and (2) angle i using Snell's law,

$$i_j = \sin^{-1} (V_{Pe})_j \sin(i_0)/V_{Po}, \quad (5)$$

where the angle of incidence i_0 is an appropriate angle for the upper crust for an epicentral distance of 55°, which is

Table 1
Crustal Velocity Models beneath KNET

Depth (km)	V_P (km/sec)	
	Chu Depression	Kyrgyz Ridge
0–3	4.90	5.50
3–7	5.50	5.90
7–17	6.20	5.95
17–27	6.50	5.95
27–38	6.70	6.30
38–50	6.85	6.85

From Ghose *et al.* (1998).

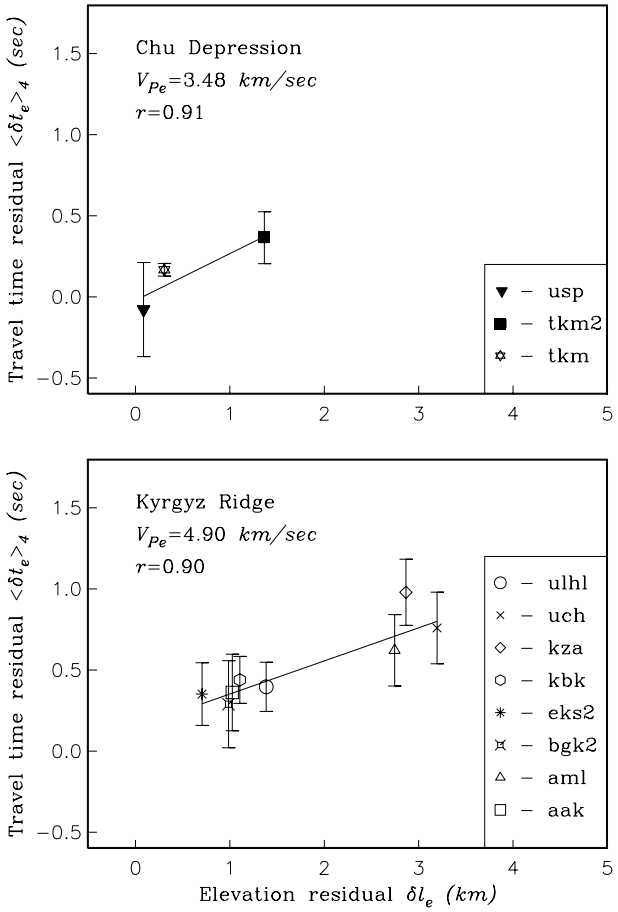

Figure 2. Elevation dependence of the *P*-wave travel-time residual $\overline{\delta t}_e$, which is the mean of four station values of $\langle \delta t_{a(st)} - \delta t_{a(chm)} \rangle_n$, where "chm" and "st" indicate δt_a at reference station CHM and any KNET station, respectively, and n is the number of measurements in an azimuthal quadrant (northeast, southeast, southwest, or northwest). Standard deviation limits are shown. Elevation travel path residual $\delta l_e = [h_{e(st)} - h_{e(chm)}]/\cos(i)$, where $h_{e(chm)}$ is the elevation (0.655 km) at reference station CHM and i is the angle of incidence of the seismic wave at the station. The correlation coefficient is r.

the mean epicentral distance of our data. We find i_0 to be 18.56° for the Chu Depression and 20.93° for the Kyrgyz Ridge. After three iterations using equations (3) and (5), we found for the Chu Depression and the Kyrgyz Ridge the final *P*-wave velocity value, V_{Pe}, of 3.48 and 4.90 km/sec, respectively. According to seismic sounding results (Belousov *et al.*, 1992) the *P*-wave velocity of the unconsolidated sediment in central Asia varies from 2.5 to 4.0 km/sec. Ghose *et al.* (1998) have found for the top layer in a 1D model, mostly elevations of Kyrgyz mountains, a V_{Pe} of 4.78 km/sec. Our estimations of V_{Pe} are in a good agreement with both results. Next we calculate the distance-dependent time correction t_e for travel in the elevation crust:

$$t_e = h_e \cos(i)/V_{Pe}. \quad (6)$$

To account for regional variations in the mantle velocity structure beneath KNET, which could differ from the iasp91 model, we calculate the distance dependence of the travel-time residual corrected for travel time in elevation crust δt^*. And to reduce any bias that may result from a nonuniform distribution of events, we use the arithmetic mean values of $\delta t^*(\Delta)$ calculated from the average in northern ($270° < \text{Az} \le 90°$) and southern ($90° < \text{Az} \le 270°$) directions (Fig. 3). In this way, the travel-time residual is

$$\delta t^*(\Delta) = \sum_{m=1}^{2} \{ \sum_{n=1}^{N_m} [\sum_{k=1}^{M_{m,n}} (\delta t_a(\Delta)_{m,n,k} - t_e(\Delta)_n)/M_{m,n}]/N_m \}/2, \quad (7)$$

where m is the direction (north and south), n is the seismic station index, k is the number of measurement, $M_{m,n} > 4$ is the maximum number of measurements in the mth direction at the nth station, and $N_m \le 12$ is the number of used stations with $M_{m,n} > 4$. The single estimation of $\delta t^*(\Delta)$ is obtained from the average of 7.5° windows.

In total, the equation to estimate travel-time residuals is

$$\delta t = t_a - (t_{iasp91} + \delta t_c + t_e) - \delta t^*(\Delta). \quad (8)$$

For earthquakes with epicentral distances between 20° and 31°, the seismic rays travel through material that deviates greatly from the iasp91 model, by −1.2 to 2.5 sec (Fig. 3). To avoid potential problems due to these differences, only earthquakes at distances between 31° and 98° were used to study the azimuthal variation of δt.

We determine a best-fit curve to the travel-time residuals δt as a function of backazimuth (Az) using a nonlinear equation:

$$\begin{aligned} \delta t = A &+ [B_1 \cos(\text{Az}) + B_2 \sin(\text{Az})] \\ &+ [C_1 \cos(2\text{Az}) + C_2 \sin(2\text{Az})] \\ &+ [D_1 \cos(4\text{Az}) + D_2 \sin(4\text{Az})] \\ &= A + B + C + D. \end{aligned} \quad (9)$$

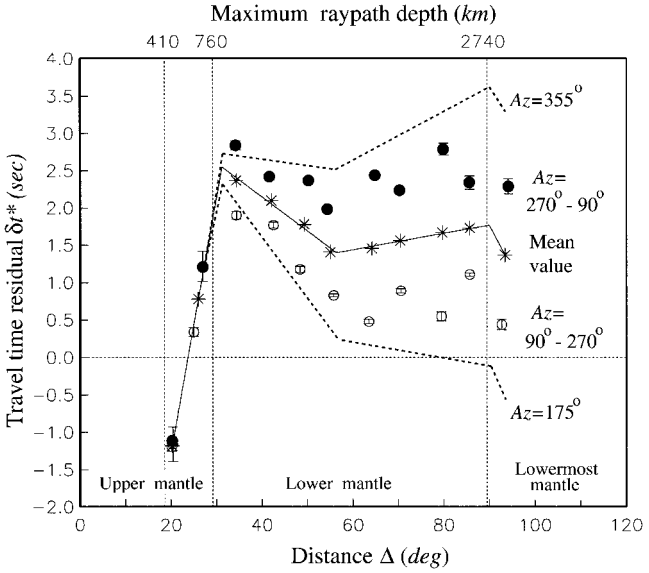

Figure 3. Distance dependence of the *P*-wave travel-time residual δt^*. For distance increments of 7.5°, the solid and open symbols are means of δt^* from waves that arrive from the north ($270° < \mathrm{Az} \leq 90°$) and south ($90° < \mathrm{Az} \leq 270°$), respectively. Standard deviations of mean are shown. The stars and solid line indicate the arithmetic mean of the northern and southern data. The dashed lines represent the distance dependence of the one-lobed amplitude variation for the fastest (Az = 175°) and slowest (Az = 355°) travel path directions of *P* waves. These dependences were calculated from mean value of δt^* (solid line) and distance dependence of *B* amplitude of δt variation (see Fig. 9a).

Backus (1965) showed that for *P*-wave propagation in a horizontal plane, a small anisotropy can be described by the sum of two- (2Az) and four-lobed (4Az) terms (*C* and *D*) that reflect the azimuthal anisotropy. The one-lobed (Az) term *B* is associated with the discontinuity slopping or lateral variation of seismic velocity. In some studies, a model of inclined anisotropic symmetry axis (Backus, 1970) is used (Babuska *et al.*, 1993; Babuska and Plomerova, 2001; Plomerova *et al.*, 2001; Bokelmann, 2002). Unfortunately, in that model it is difficult to discriminate the effect of a dipping interface versus the effect of anisotropy (Levin and Park, 1997). Nevertheless, both models give similar results for the directions of the fast and slow anisotropy axis, as it is found in North America (Dziewonski and Anderson, 1983; Bokelmann, 2002).

Results

Our models of the directional variations of the P-wave travel-time residual show a very strong azimuthal, mostly one-lobed, variation (Fig. 4; Table 2). This result is stable over all stations. The travel-time residuals each have one minimum value near Az = 180° (directly south), and two maximum amplitudes occur at ~50° and ~340°. The mean value of the maximum amplitude for the one-lobed variation is 2.7, and 5.2 times larger than for two-, and four-lobed values, respectively (Table 2). This shows that the maximum amplitude of the travel-time residual is very large, in some cases more than 5.0 sec (TKM2). The standard deviation of the azimuthal direction of the minimum and maximum amplitude is 4.8° and 4.7° for the one- and two-lobed variations, respectively. The azimuthal directions for the one- and two-lobed variations are almost identical, 175° and 179°, respectively. Uncertainties in our estimates of δt may be introduced from errors in the analysis *P*-wave arrival time pick, data measurements, or initial processing errors or the results of the location presented in the PDE bulletin. The high correlation coefficient r^* (Table 2) demonstrates that there is a good fit between the model and our data, yet these correlation results primarily apply to the one-lobed variation that predominates.

To study the azimuthal variations in travel-time residuals, we have developed an additional technique for measuring uncertainties of the two- and four-lobed variations using results from station KZA (Fig. 5c shows a schematic of our technique). Using a Monte Carlo simulation, we generate synthetic data sets by randomly converting observed backazimuths Az_j and travel-time residuals $\delta_3 t_j$ ($=\delta t - \delta t(A,\mathrm{Az})$), where j ($= 1, \ldots, 17$) is the number of azimuthal windows used for station KZA (Fig. 4). From these synthetic data and equation (9), we can derive corresponding synthetic amplitudes C^* and D^*. From 1000 synthetic data sets, we calculate the mean of the maximum amplitudes for the two- and four-lobed variations and their standard deviations: $\langle C^*_{\max}\rangle \pm s$ and $\langle D^*_{\max}\rangle \pm s$ (or $\langle |C^*_{\min}|\rangle \pm s$ and $\langle |D^*_{\min}|\rangle \pm s$). These parameters, normalized by our experimental data, are statistical estimations of the noise. We find that there is about a 68% chance that the two-lobed model (Fig. 5d) fits these data correctly. A Student's test (Press *et al.*, 1986) of the experimental and synthetic means, $\langle C_{\min}\rangle_9$ and $\langle C^*_{\min}\rangle_9$ (Table 2), shows that the difference of these means is statistically very significant.

We performed the same statistical tests on the four-lobed pattern variations. We found that the fit between our data and the model was poor statistically and equivalent to the amplitude of noise (Fig. 5e; Table 2). This is a very common result that many authors have found in studies of P_n velocity anisotropy (e.g., Morris *et al.*, 1969; Crampin and Bamford, 1977; Vetter and Minster, 1981). At the same time, we find amplitude dispersion is practically 2 times less in the data than in the synthetic. Because both the two- and four-lobed variations were tested using data from station KZA, we conclude that our results from the two-lobed pattern are robust to measurement errors, whereas the four-lobed pattern is not. We do not include the four-lobed term in our determination of the direction of anisotropy but do include it in our calculations of two- and four-lobed distance dependence.

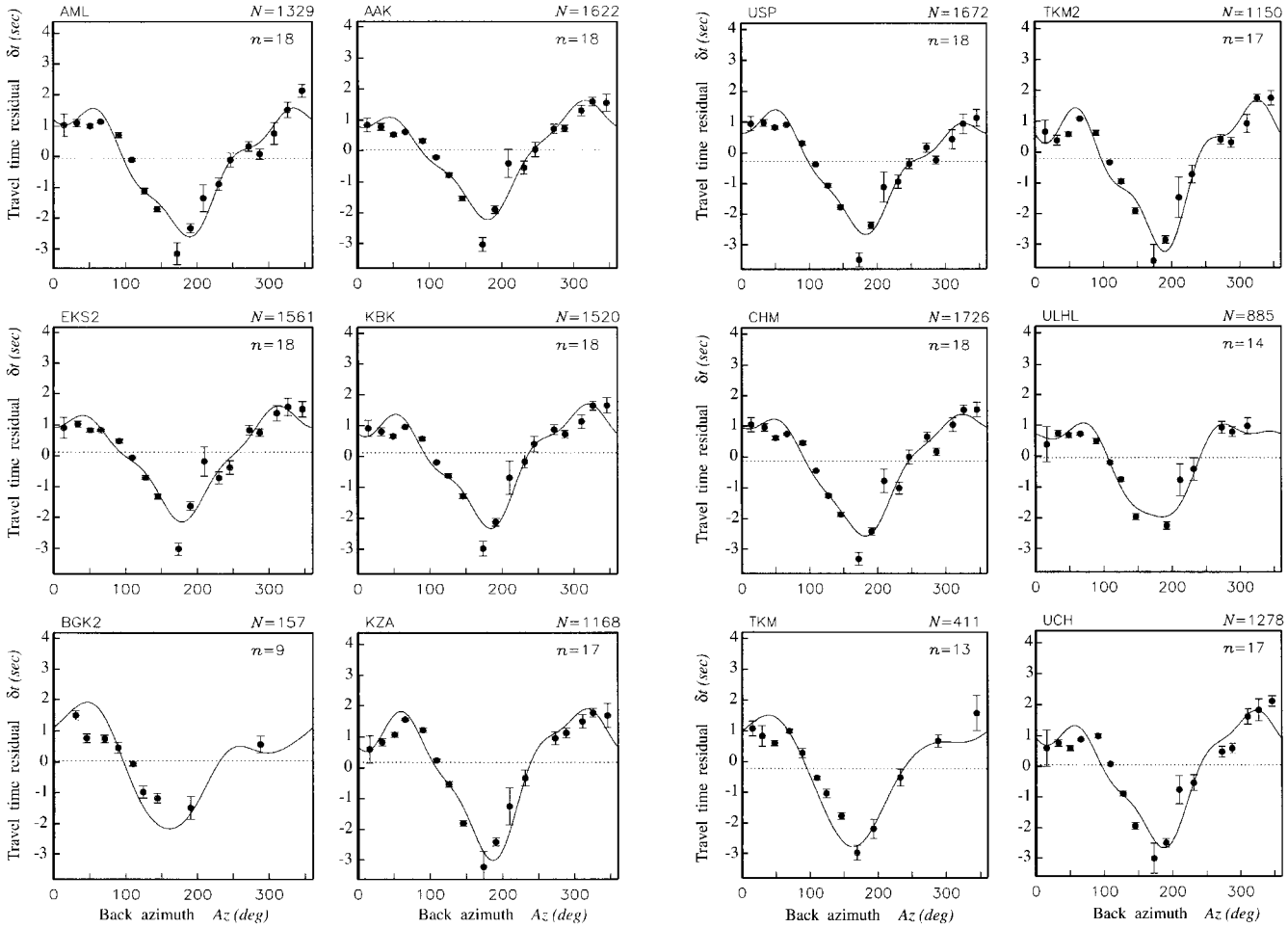

Figure 4. *P*-wave travel-time residuals δt and curves that modeled the sum of one-, two- and four-lobed (Az, 2Az, and 4Az) directional variation of δt. Each point is a mean value (greater than four arrivals) of δt in azimuthal windows 20° wide. For each station, we list the number of points (n) and the number of arrival times (N). Standard deviations of mean are shown, but means are treated with equaled weight (Herrin and Taggart, 1968; Dziewonski and Anderson, 1983). The dashed line is the least-squares fit of the constant term A (equation 9). Data from stations BGK2, TKM, and ULHL do not cover the entire range of azimuthal directions ($n < 17$), so no results were obtained for these stations.

Interpretation

Azimuth-Independent Parameter *A*: Moho Depth Variation

The mean values of term A in equation (9) show that the *P*-wave arrivals at KNET stations in the Chu Depression, -0.20 ± 0.06 sec (Table 2), are faster than in the Kyrgyz Ridge, 0.06 ± 0.08 sec. We believe that variation of the azimuth-independent term A results from the Moho depth variations. The northern Tien Shan (Kyrgyz Ridge) is bordered over the Chu Depression by the Kazakh Shield (Sadybakasov, 1990), and according to Sabitova (1978, 1986) the crustal thickness varies from 45 km (Kazakh Shield) to 55 km (northern Tien Shan). The Moho depths estimated by receiver function analysis (Bump and Sheehan, 1998; Oreshin *et al.*, 2002; Vinnik *et al.*, 2002b) and Rayleigh-wave dispersion (Mahdi and Pavlis, 1998) confirm that the crust beneath the Kazakh Shield is about 10 km thinner than below the northern Tien Shan. For both geological structures, the Chu Depression and the Kyrgyz Ridge, we suggest the Moho depth h_M is 50 km (Table 1). From the velocities of 6.85 km/sec (upper Moho discontinuity) and 8.04 km/sec (below Moho), the results on term A give the variation of h_M (Fig. 6) to be ~11 km, from 41.9 ± 2.5 to 52.6 ± 3.4 km with regard to the reference value of h_M ($=50$ km).

A 3D velocity model (Ghose *et al.*, 1998) shows that the structure boundary between the Chu Depression and the Kyrgyz Ridge is close to the strike of the Kyrgyz Ridge (east–west direction), below stations EKS2, BGK2, AAK, and KBK. This zone is recognized as an area of crustal thickness variations in the north–south direction in the δt_k(Az) results. A value of δt_k is a travel-time residual δt_e (equation

Table 2
Directional Variations of Travel-Time Residuals

Seismic station	Term A (sec)	One-lobed term		Two-lobed term		Four-lobed term		$r^{*\S}$
		B_{max} (sec)	Az (deg)*	$\|C_{min}\|$ (sec)	Az (deg)†	$\|D_{min}\|$ (sec)	Az (deg)‡	
AML	−0.05	1.85	2	0.48	−4	0.33	18	0.91
UCH	0.05	1.78	−9	0.71	4	0.34	14	0.87
EKS2	0.12	1.54	−6	0.48	2	0.26	−2	0.88
BGK2	0.05							
AAK	0.05	1.55	−11	0.51	3	0.26	4	0.89
KBK	0.14	1.55	−9	0.62	1	0.37	10	0.90
KZA	0.19	1.81	−4	1.05	2	0.40	12	0.93
ULHL	−0.04							
USP	−0.27	1.65	3	0.53	−10	0.29	9	0.91
CHM	−0.12	1.78	−6	0.51	−4	0.21	10	0.90
TKM	−0.22							
TKM2	−0.19	1.85	−5	0.80	3	0.52	16	0.90
Mean value		1.71 ± 0.13	−5.0 ± 4.8	0.63 ± 0.19	−0.3 ± 4.7	0.33 ± 0.09	10.1 ± 6.1	
Simulation data				0.27 ± 0.14		0.29 ± 0.16		

*Azimuthal direction (from north) for maximum time delay $B_{max} = B_1 \cos(Az) + B_2 \sin(Az)$; the direction of minimum value B_{min} is determined by adding of π.

†Azimuthal direction for $C_{min} = C_1 \cos(2\,Az) + C_2 \sin(2\,Az)$; another direction of minimum value is determined by adding of π.

‡Azimuthal direction for $D_{min} = D_1 \cos(4\,Az) + D_2 \sin(4\,Az)$; other directions of minimum value are determined by adding of $k\pi/2$, where $k = 1, 2, 3$.

§Correlation coefficient $r^* = ((s_y^2 - s_e^2)/s_y^2)^{0.5}$, where s_y is the standard deviation of δt from all estimates (number $n \leq 18$) and s_e is standard deviation of the curve modeled azimuthal variations δt.

2) in an azimuthal quadrant corrected for travel time in the station's elevation t_e (equation 6):

$$\delta t_k = \sum_{j=1}^{M_k} (\delta t_e)_j / M_k - t_e + c, \qquad (10)$$

where k is the quadrant number, j is the measurement number, M_k is the maximum number of measurements in the kth quadrant, and c is the constant to account for the 0.05-sec travel time through material above 0-km elevation at reference station CHM. The Student's test of the δt_k for different quadrants shows that in most of the cases, the observed differences of δt_k are very significant. One reasonable explanation of the mapped directional variations in δt_k (Fig. 7) is crustal thickness variations across the structural boundary.

The north–south direction of h_M variation is reflected in the amplitude results, B_{max} ($= |B_{min}|$) obtained for the one-lobed azimuthal variation of δt (Table 2). Seismic stations EKS2, AAK, and KBK located in the structure boundary zone (Fig. 8a) have the smallest values of B_{max} ($= 1.55 \pm 0.06$ sec). In contrast, the mean value of B_{max} at two stations near the Chu Depression (CHM, TKM2) equals 1.81 ± 0.04 sec. The same value of B_{max} was obtained from other stations near the Kyrgyz Ridge (AML, UCH, and KZA): 1.81 ± 0.04 sec. For the slowest northern path (B_{max} direction), delay times (Fig. 8b) estimated from terms A and B_{max} (Table 2) for stations near the Chu Depression (δt_{n1}) and the anomalous zone, (δt_{n2}) are approximately equal (1.65 ± 0.01 and 1.64 ± 0.05 sec). But for the fastest southern path (B_{min} direction), times δt_{s1} ($= -1.97 \pm 0.10$ sec) and δt_{s2} ($= -1.44 \pm 0.05$ sec) are significantly different, 0.53 sec. In part (~0.17 sec), this is due to different velocity structures (Table 1; Fig. 8a). For the additional difference of 0.36 sec, the most likely explanation is that the Moho is depressed toward the south near stations EKS2, AAK, and KBK. Below the Kyrgyz Ridge, a value of h_M reaches 58 km; it is about 4 km bigger than the obtained estimation from the mean value of term A (AML, UCH, KZA).

Azimuth-Dependent One-Lobed Parameter B: Lower Mantle Velocity Variations

The northern and southern directions for the slowest and fastest P-wave travel times were identified for events located more than 30° away when we estimated the δt^* dependence on epicentral distance (Fig. 3). The features of δt^* (Δ) are associated with the mantle structure variations with regard to the iasp91 model. We investigated the amplitudes of one-lobed, and sum of two- and four-lobed azimuthal variations as a function of distance and depth using five iterations of a two-step calculation. In the first step, a value of travel-time residual δt was determined after the elimination of two- and four-lobed distance dependence; the variations were normalized by the one-lobed variation amplitude (Fig. 9a),

$$B_{r_n}(\Delta) = \sum_{i=1}^{9} \sum_{j=1}^{M_i} [\delta t_{i,j}(Az,\Delta) - A_i - (C_i + D_i) \times C_{r_{n-1}}(\Delta)]/B_i, \qquad (11)$$

where i is the seismic station index (Table 2), j is the measurement index at ith station, M_i is the maximum number of measurements at ith station, n is the iteration index, and A_i,

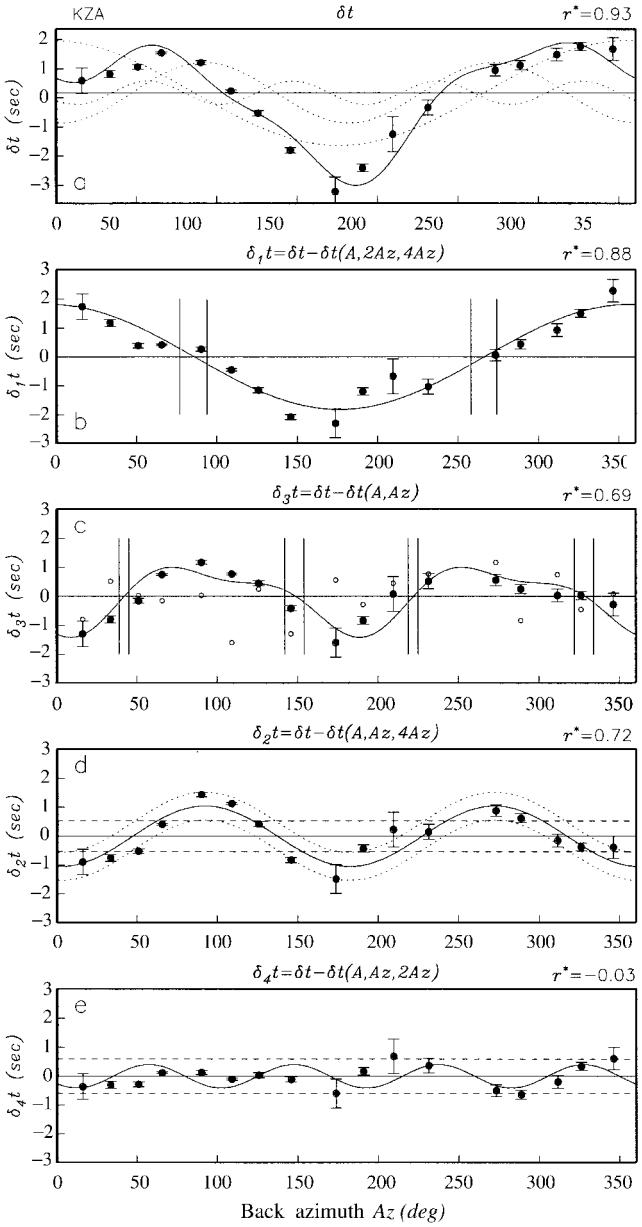

Figure 5. Travel-time residual δt for station KZA as a function of backazimuth Az. Uncertainty estimates of the standard deviation limits of the mean are shown, and the correlation coefficient r^* (see definition in Table 2) titles each subfigure. (a) Travel-time residuals δt and model curves for one-, two- and four-lobed (dashed lines) and their sum (solid line) azimuthal variations. (b) One-lobed variation of *P*-wave travel-time residual. Azimuth-independent term A and two- and four-lobed variations are subtracted from observed results on δt. Vertical lines (significance of threshold κ) indicate the azimuthal windows around $\delta_1 t$ ($=0$) not used in the study of distance dependencies of B_r amplitude of variation (see Fig. 9 and explanation in text). (c) Two- and four-lobed variations. Term A and one-lobed variation are subtracted from δt. Open circles depict one of our Monte Carlo simulations of mixed $\delta_3 t$ and Az data. Vertical lines indicate the azimuthal windows around $\delta_3 t$ ($=0$) not used in the study of distance dependencies of C_r amplitude of variation (see Fig. 9 and explanation in text). (d) Two-lobed variation (solid line). Term A and one- and four-lobed variations are subtracted. The 68% confidence intervals (dotted line) are shown. Horizontal long-dashed line is the sum of the mean of two-lobed amplitude variations plus standard deviation estimated from 1000 sets of synthetic data of $\delta_2 t$. (e) Four-lobed variation (solid line). Term A and one- and two-lobed variations are subtracted. Horizontal long-dashed line is the sum of the mean of the four-lobed amplitude variations plus standard deviation estimated from 1000 sets of synthetic data of $\delta_4 t$.

B_i, C_i, and D_i are amplitudes of the azimuth-independent term and one-, two-, and four-lobed azimuthal variations (equation 9) at ith station. For the first iteration, C_{r0} equals 1.0.

In the second step, δt was normalized by the sum of the two- and four-lobed variations after elimination of the one-lobed distance-dependent variation (Fig. 9b),

$$C_{r_n}(\Delta) = \sum_{i=1}^{9} \sum_{j=1}^{M_i} [\delta t_{i,j}(\mathrm{Az},\Delta) - A_i - B_i \times B_{r_n}(\Delta)]/(C_i + D_i). \quad (12)$$

To avoid singularities that occur when the B and (C + D) values are small, we did not use any data that had a normalization factor that was less than a threshold value κ, which we set to 0.14. This value was estimated from the ratio of $|B|/B_{\max}$ and $|C + D|/|(C + D)_{\max}|$ and was also based on the maximum value of the correlation coefficient (Fig. 9c) attained between the distance and logarithm of the normalized one-lobed amplitude variation (Fig. 9a).

Based on the distance-dependence results of δt^* (Fig. 3) and the amplitude of the one-lobed variation (Fig. 9a), we modeled the distance dependencies of travel-time residuals for two directions (Fig. 3): for the slowest direction (north) and for the fastest direction (south). From the southern (Az = 175°) and northern (Az = 355°) distance dependencies of δt, we calculate the regional velocity structure as the correction coefficients to reference model iasp91. These dependencies are identical in the distance range 20°–29° away from the station and for turning depths of ~415–660 km. Since we lack data in distance ranges $\Delta < 20°$, we assume

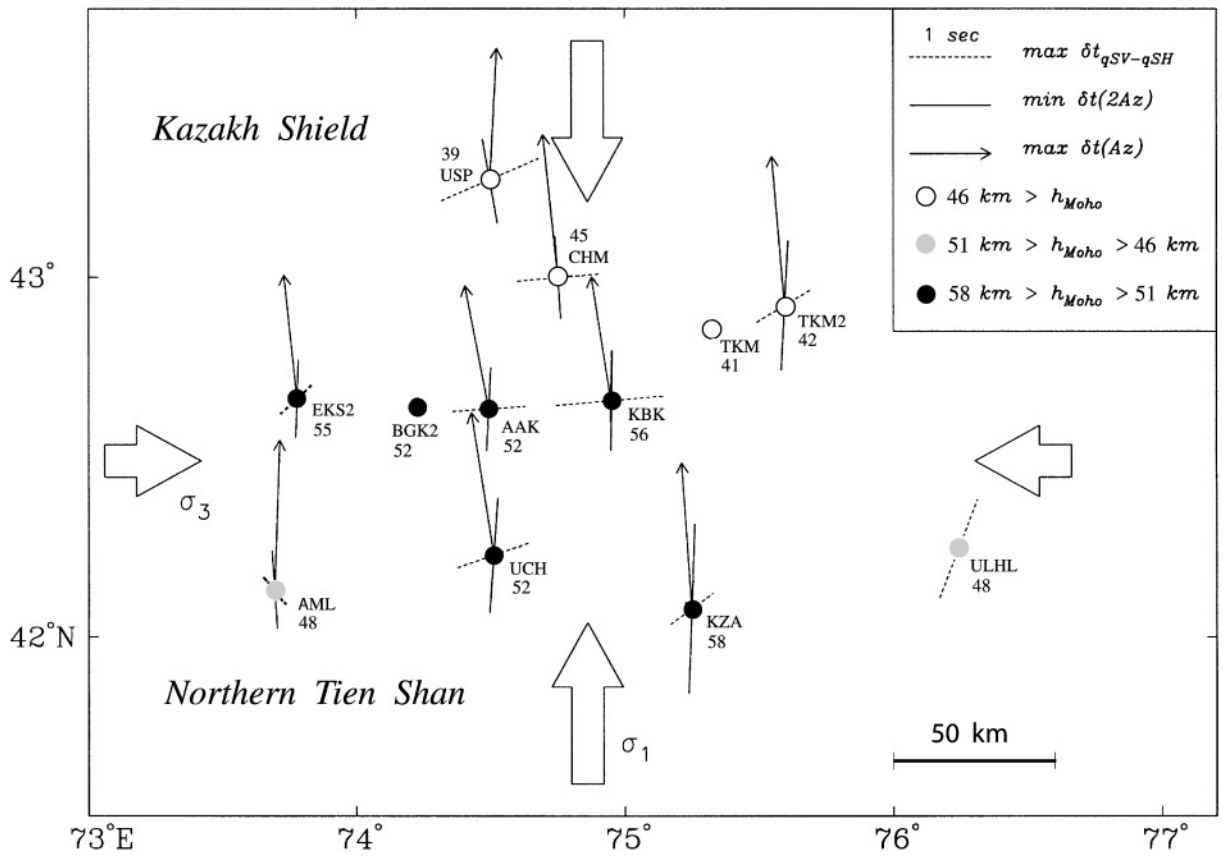

Figure 6. Azimuthal variation of *P*-wave travel-time residual. The dashed line represents the shear-wave splitting results showing the direction of polarization of the fast component (*qSV* or *qSH*) of *SKS* waves (after Wolfe and Vernon, 1998). The lengths of the lines are proportional to the magnitude of the delay time $\delta t_{qSV\text{-}qSH}$ and amplitude of the azimuthal variation of δt. The solid line and thin arrow show the directions of one- (Az) and two-lobed (2Az) variations of the *P*-wave travel time. The length of this line is proportional to the amplitude. Open, gray, and filled circles represent the estimates of Moho depths obtained from the azimuth-independent term *A*; numbers are crustal thickness with regard to the reference value of Moho depth, 50 km. Large arrows indicate the directions of the principal axes of the force system in the source from mechanisms of local earthquakes in the crust of the northern Tien Shan (after Junga [1990]).

that in the vicinity of KNET, the velocity structure is uniform for depths between 50 and 415 km. Above the 415-km discontinuity, the compressional wave velocity is faster than the reference model by 1.5% (Fig. 10). This result disagrees with the present image of low-velocity structure in the uppermost mantle beneath the northern Tien Shan (Vinnik and Saipbekova, 1984; Roecker *et al.*, 1993; Mahdi and Pavlis, 1998; Oreshin *et al.*, 2002). The maximum ray path depth sampled by $\delta t^*(\Delta)$ on distance 20° is ~415 km, and we can estimate only a mean value of V_P for depths between 50 and 415 km. At the same time, the upper mantle structure beneath central Eurasia (model CE2000) determinated from *P* waveforms from explosions at a nuclear test site in Kazakhstan is ~0.7% faster than the iasp91 model (Goldstein *et al.*, 1992). One of the seismic stations whose data were used for model CE2000, GAR, was located on the southern border of the Tien Shan and the seismic ray path crossed the upper mantle beneath KNET. Synthetic waveforms produced by model CE200 are in a good agreement with data from station GAR.

For earthquakes at larger distances, and depths from 415 to 774 km, the *P*-wave velocity model is 1.7% slower than the iasp91 model. The results of the inversion of shear and surface waveforms confirm the presence of a low-velocity zone under the Tien Shan at depths from 300 to 600 km (Friederich, 2004). In the southern direction, named earlier, the fastest compressional wave velocity for depths more than 774 km is consistent with the iasp91 model. It is clear that the low-velocity structure is situated north of KNET. We modeled the low-velocity zone as an anomaly that is 1.5%–2.0% slower than the iasp91 model. In this model, the low-velocity structure extends a distance of ~18.7°–29.4° in the northern direction and to lower mantle depths of 2200–2600 km.

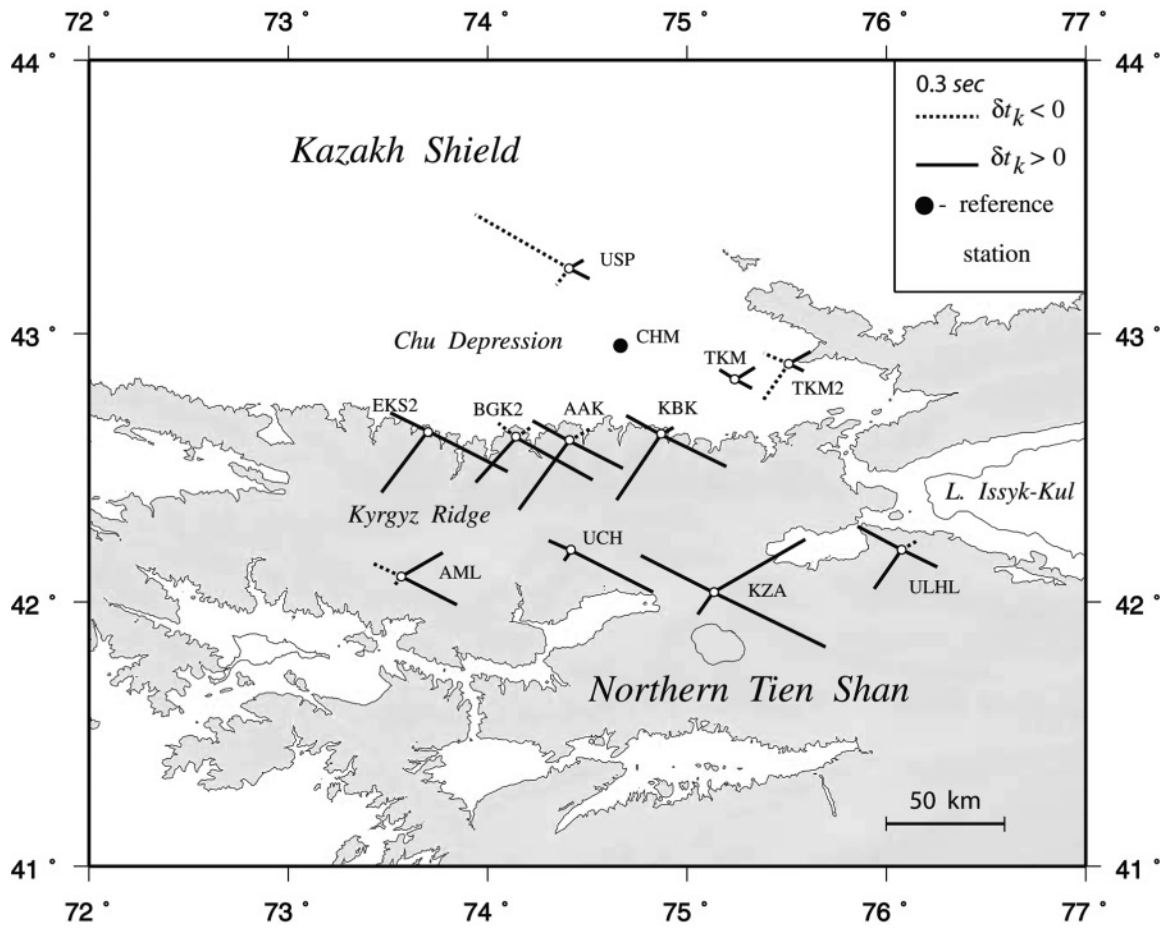

Figure 7. Directional variations of travel-time residual δt_k, estimated as travel-time differences with respect to reference station CHM. An azimuthal quadrant's value of δt_k is a travel-time residual δt_e (equation 2) corrected for travel time in the station's elevation t_e (equations 6 and 10).

Azimuth-Dependent Two-Lobed Parameters *C*, *D*: Mantle Anisotropy

The fast *P*-wave travel-time directions of the two-lobed variation indicate that the azimuthal anisotropy in the mantle is north–south (Table 2; Fig. 6). Using the results of the two- and four-lobed distance-dependent variations (Fig. 9b), we estimate an ~440-km thickness of the anisotropic layer, which extends to the top of the lower mantle. From *P*-wave travel-time t_{al} estimates and the amplitude of the sum of the two- and four-lobed δt variations associated within the anisotropic layer, we estimate the velocity anisotropy $\delta V/V$ as $|(C + D)_{max}|/t_{al}$ to be ~2.0%–2.9%.

The slowest *P*-wave travel-time directions of the two-lobed variation (Fig. 6) suggest that the azimuthal anisotropy in the mantle is slowest at 89.7° and 269.7° ± 4.7° (almost east–west). This orientation is close to the strike of the mountain belt within the northern Tien Shan. Makeyeva *et al.* (1992) and Wolfe and Vernon (1998) mapped the mantle strain in the northern Tien Shan (Fig. 6) using a shear-wave splitting method based on *SKS*, and *SKKS* waves. They found the fast polarization direction to be parallel to the strike of the deformation zone over the northern Tien Shan (~east–west). The result of Helffrich *et al.* (1994), which used *S*-wave data from station AAK, also confirms this conclusion.

Discussion

From shear-wave splitting analyses, it is often inferred that the main cause of the anisotropy is the preferred orientation of olivine during shear deformation in the presence of finite strain. For example, Makeyeva *et al.* (1992) interpreted the anisotropy to be a result of uniaxial compression of olivine-rich rock deformation. Alternatively, the model created using KNET data proposed by Wolfe and Vernon (1998) suggests pure shear deformation. Both of these models contradict our results of an azimuth dependence of the *P*-wave travel-time residual, with the general tendency of the fastest direction to be −0.3° ± 4.7° (north) and 179.7° ± 4.7° (south).

The *SKS* splitting method cannot be used to predict the depth of the anisotropic layer. Nevertheless, it is expected

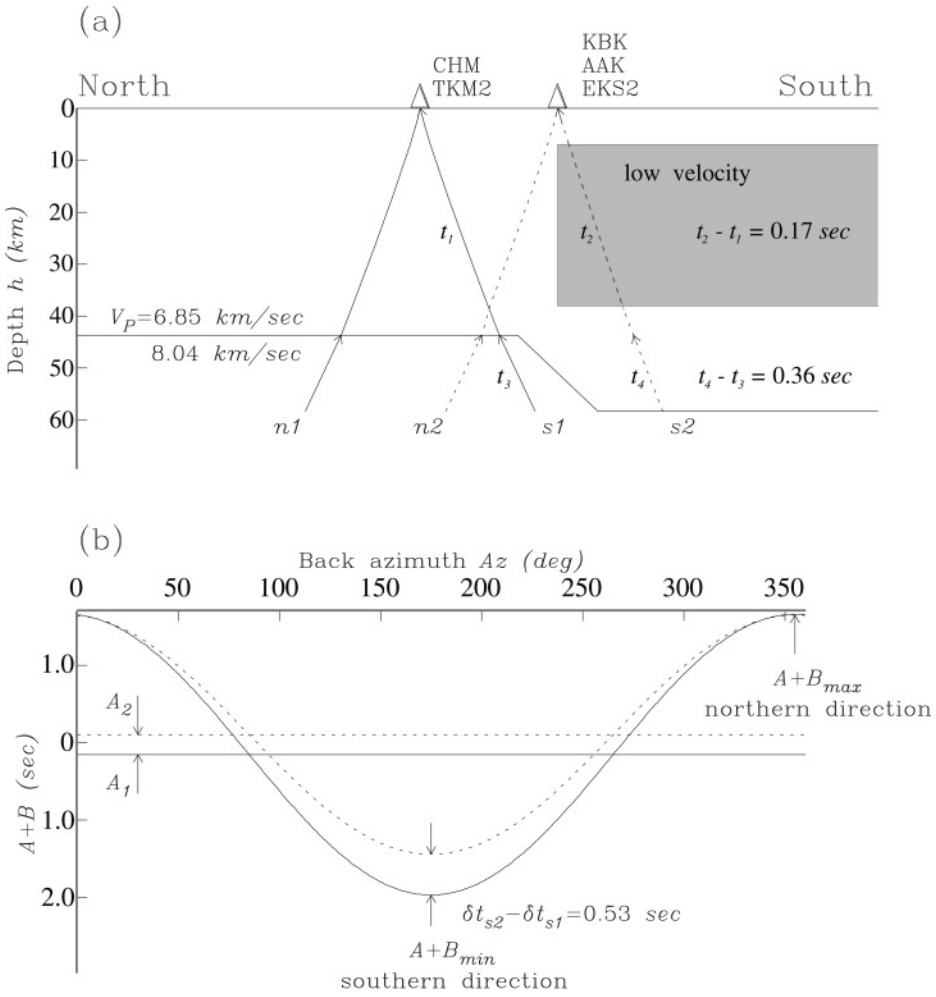

Figure 8. Cartoon showing (a) the propagation path across the Moho discontinuity beneath KNET stations and (b) the influence of the Moho depth variation on the amplitude of the one-lobed term B (Table 2). The dotted line on (a) represents a path to stations situated in a zone of crustal thickness variation in the north–south direction from 43.7 to 58.3 km. The dotted line on (b) shows a one-lobed variation of δt for stations in the anomaly zone of the Kyrgyz Ridge (EKS2, AAK, and KBK), and the solid line represents the same variation from outside the area, in the Chu Depression. A_1 and A_2 are the mean values of the azimuth-independent term A obtained for the Chu Depression and anomaly zone (EKS2, AAK, and KBK), respectively. t_1, t_2 and t_3, t_4 are the travel times in the ranges of depths 43.7–0.0 and 58.3–43.7 km, respectively.

that there is some anisotropy in the upper mantle. In some cases, this point is based on results of 3D splitting variations (Silver *et al.*, 1989) or combining results of *SKS* and *P* receiver functions (Vinnik *et al.*, 2002). It is apparent that the azimuthal anisotropy based on *P*-wave travel-time variation and shear-wave splitting has different depths and different sources. From this, we expect there are two anisotropy layers for the northern Tien Shan. But Wolf and Vernon (1998) did not find any indication of a two-layer model of anisotropy. A source of this discrepancy could be in the different frequency bands of the analyzed seismic waves (Marson-Pidgeon and Savage, 1997; Liu *et al.*, 2001). Teleseismic *P* waves in our research have a predominant period of about 1 sec, whereas the period of *SKS* waves used in the splitting method varies from 6 sec (Wolf and Vernon, 1998) to 8–15 sec (Makeyeva *et al.*, 1992). If we assume a different predominant orientation of anisotropy sources, with different scales, then the anisotropy effect should be mostly produced by anisotropy inhomogeneities that scale with wavelength.

Babuska *et al.* (1993) proposed the seismic anisotropy was a 3D phenomenon and derived models from *P* and *SKS* data. These models have a common anisotropy root, and the authors suggested that a bipolar pattern (one-lobed variation in our interpretation) of the *P*-wave travel-time residuals reflects an inclination of the symmetry axes of the olivine aggregates. Bormann *et al.* (1993) noticed that the bipolar model proposed by Babuska *et al.* (1993) for central Europe gives incompatible thicknesses of the anisotropic layer: be-

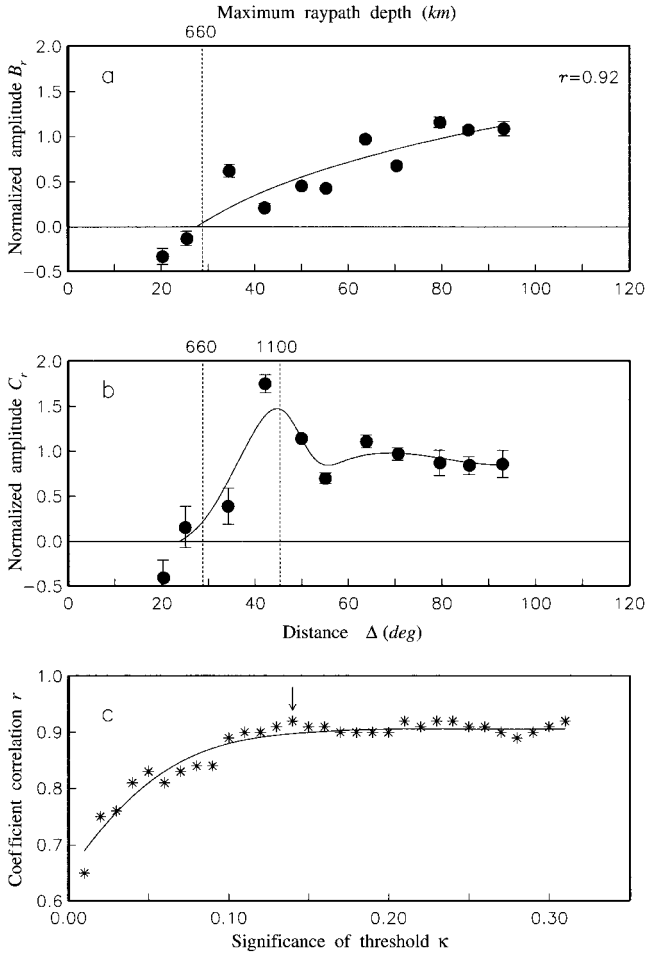

Figure 9. Distance dependence on the azimuthal amplitude variation. (a) B_r is one-lobed variation amplitude of δt, normalized by the amplitude of B obtained for $\Delta \geq 31°$ after subtraction of azimuth-independent term and two- and four-lobed distance-dependent variations. (b) C_r is a sum of two- and four-lobed variation amplitudes $C + D$ obtained for $\Delta \geq 31°$ after subtraction of azimuth-independent term and one-lobed distance-dependent variation. (c) Illustration of how we select minimum value of the significance threshold, which we use as a normalization factor δt(Az) and δt(2Az, 4Az) (see Fig. 5b,c).

tween 180 and 2500 km from shear-wave splitting data and between 130 and 200 km from azimuthal variations of δt_P. From KNET data, our results find that the one-lobed variation is best modeled with a low-velocity structure in the lower mantle north of KNET. Some global travel-time tomography results (Van der Hilst *et al.*, 1997; Bijward *et al.*, 1998) demonstrate the presence of a lateral discontinuity in the lower mantle near central Asia that traverses KNET in the ~east–west direction. Just north of this boundary is a low-velocity region. The amplitude of the velocity variation with respect to the reference velocity model ak135 is −0.5% (Bijward *et al.*, 1998).

It was noted that one of the main features of the lateral variation in the lower mantle is the corresponding high-velocity anomalies within the high-velocity subduction zones in the upper mantle (Van der Hilst *et al.*, 1997). At the same time, connection of low-velocity anomalies in the lower and upper mantle across the 660-km discontinuity was observed below Iceland, Hawaii, and the South Pacific, regions with spreading tectonic and in some cases regions with intraplate stress, such as incipient continental rifting in East Africa (Bijward *et al.*, 1998; Zhao, 2001; Shen *et al.*, 2002). All these regions are associated with hotspots (small areas of volcanism or high heat flow). One explanation of the hotspot origin is a plume model (Morgan, 1971). A plume is a narrow area (conduit) of upwelling of low-viscosity hot magma that originates at the core–mantle boundary. From model experiments (e.g., Griffiths and Campbell, 1990), the size of a plume head was estimated to be 1000 km at the core–mantle discontinuity and 2000 km beneath the lithosphere. Olson (1987) suggested that the trace of the plume can deviate from vertical because of the large-scale convection of mantle material. In this way, the direction of plume tilt can be both coherent to plate motion as well as opposite to it. This last scenario is possible if the viscosity in the upper mantle is very low (see figure 3 of Steinberger and O'Conell, [1998]).

As in Figure 10, a core–mantle discontinuity could be a place of origin for low-velocity anomaly if it is about −1.4%. The dimension of the anomaly we find in the north–south direction is ~600–1000 km. The structure is tilting in the southern direction, whereas the plate motion direction is north. Steinberger (2000) calculated the present-day mantle flow at the top of D″ and the depth of 670 km. He found that the model viscosity in the upper mantle was about 100 times less than in the lower mantle. The tilt of this anomaly zone is consistent with the directions of flow model in the lower mantle beneath the northern Tien Shan. Some of our observations are consistent with the typical features of a plume. As for the absence of a trace of the conduit (low-velocity zone) in the upper mantle, we suggest a possible scenario. If mantle flow strongly varies with depth around the 660-km discontinuity (Whitehead, 1982), the plume might not reach the Earth's surface but instead intrude into the middle mantle.

We find the fastest direction of the azimuthal anisotropy of the *P*-wave travel time is parallel to the absolute motion of the India plate. The agreement between the anisotropic fast axes obtained from *P*-wave travel times and the absolute plate motions is excellent (Dziewonski and Anderson, 1983; Bokelmann, 2002). We find that one of the fastest directions of the azimuthal anisotropy of the *P*-wave travel time is close to the updipping direction of the low-velocity zone, which trends 179.7° (north–south). Vinnik (1989) noticed that in some regions the 660-km discontinuity could be replaced by an equivalent gradient layer about 100 km or thicker, which could be anisotropic (Muirhead, 1985). Later Vinnik and Montagner (1996) and Vinnik *et al.* (1998) demonstrated evidence for anisotropy at the bottom of the upper mantle

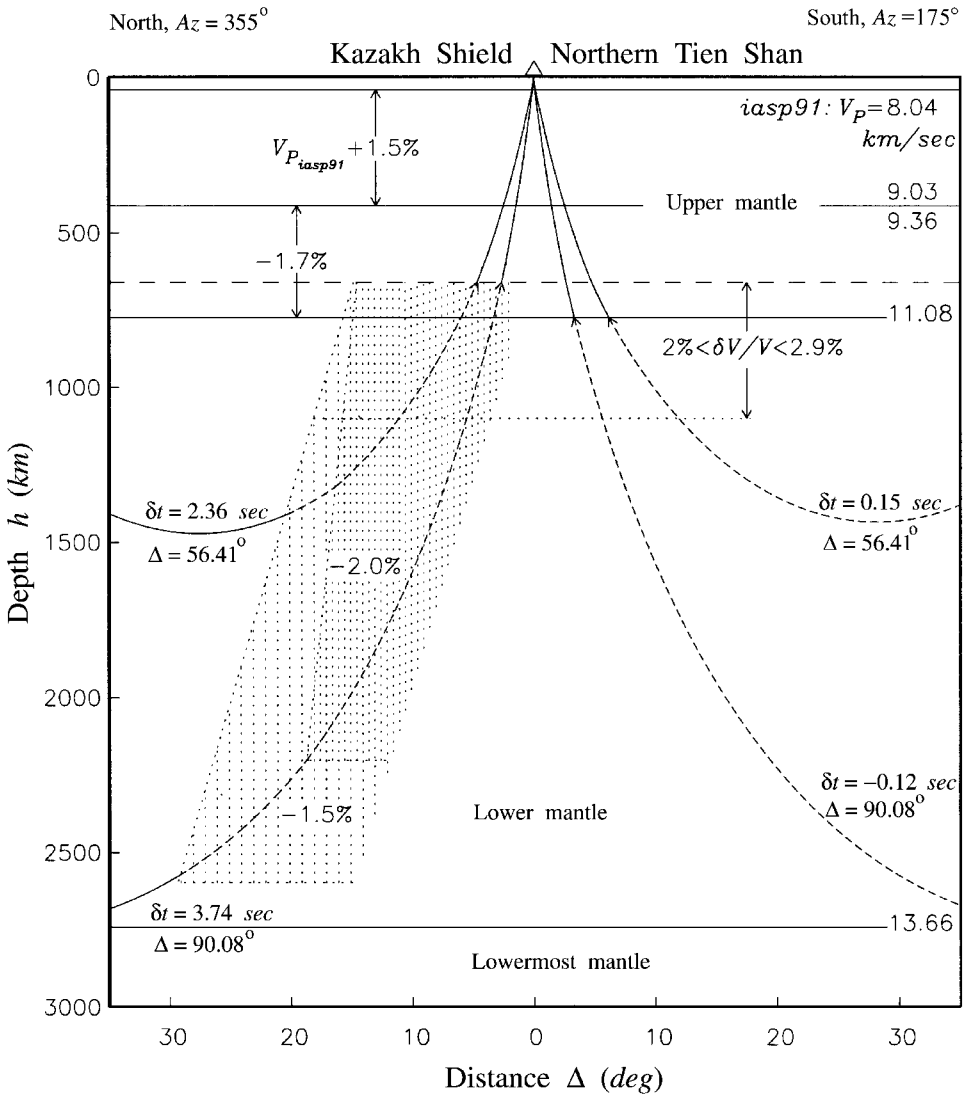

Figure 10. Model that is representative of the results we obtained from our study of azimuthal variations in the *P*-wave travel-time residuals for the most fast and slow directions (see Fig. 3). There are given for the northern direction two examples of low-velocity zones as anomalies with magnitudes of −1.5% and −2.0%. Dashed line represents a ray path through the structure that accounts for the delay time δt. For the northern direction, it is a velocity anomaly with a magnitude of −1.5%.

beneath central Africa. Montagner and Kennet (1996) and Wookey *et al.* (2002) also recognized the presence of anisotropy in a mid-mantle boundary layer, in the vicinity of the 660-km discontinuity.

The origin of the anisotropy in the lower mantle beneath the northern Tien Shan is not clear. The interpretation of seismic anisotropy in the uppermost mantle refers to lattice-preferred orientation of olivine, $(Mg,Fe)SiO_4$, in material that is deformed by dislocation creep. With increasing pressure at depth ~660 km after a few phase transformations, olivine converts to magnesiowustite, (Mg,Fe)O. One idea is that (Mg,Fe)O explores the anisotropy in the lower mantle (Karki, 1997; Yamazaki and Karato, 2004). Using numerical modeling, McNamara *et al.* (2002) have shown that dislocation creep could be caused by high stress associated with the collision of a subducted slab with the core–mantle boundary. And this results in lattice-preferred orientation of magnesiowustite with anisotropy ~1%–2%. An alternative interpretation proposes the shape-preferred orientation of elastically heterogeneous materials (Kendall and Silver, 1996). Wookey *et al.* (2002) discussed models of anisotropy bellow 660 km associated with slab material pooling in the lower mantle. It might be possible that the azimuthal anisotropy we find in this study is induced by horizontal hot flow recognized as a head plume intruded at the top of the lower mantle.

Conclusions

In this study, using *P*-wave travel-time residuals, we found a low-velocity zone in the lower mantle beneath the Kazakh Shield. A velocity model anomaly with a magnitude of about −1.5% in this zone is consistent with upwelling of a mantle plume. Here, we assume the plume source depth is the core–mantle boundary and that the plume conduit is tilting in the southern direction opposite to plate motion such that the head plume material pooled in the vicinity of the top of the lower mantle. This anisotropy layer is situated between the 660-km discontinuity and a depth of 1100 km. The anisotropy is inhomogeneous. The magnitude of the peak-to-peak amplitude for the two-lobed term noticeably varies (Table 2) from the west to the southeast: from 1.00 ± 0.04 sec (AML, AAK, EKS2, USP, and CHM) through 1.33 ± 0.13 sec (UCH and KBK) and 1.85 ± 0.35 sec (KZA and TKM2). One of the fastest directions, Az = 179.7°, of the azimuthal anisotropy (2.0%–2.9%) follows the assumed upwelling direction, Az = 175°. We suggest that the azimuthal anisotropy may be due to the shape-preferred orientation of large elastic inclusion that results from the plume intrusion. The fast anisotropy direction reflects the direction of a large-scale mantle convection the agreement between the anisotropic fast axis and absolute India's plate could be indicative of this relationship. For the upper mantle, between 415 and 774 km a relatively simple model suggests that the velocity is 1.75% slower and between 50 and 415 km is 1.5% faster than the reference model iasp91. The crustal thickness below the Kazakh Shield is about 11–15 km thinner than beneath the northern Tien Shan.

Acknowledgments

We appreciate the efforts of G. Offield, J. Eakins, and J. Tytell. We thank IVTAN, KIS for operation of the KNET network and IRIS for supporting KNET. We are grateful to Rob Mellors for his careful review of the article, with many helpful suggestions, and to Garry Pavlis for constructive discussion. This work was supported by NSF Grant No. EAR9614282.

References

Abdrakhmatov, K. Ye., S. A. Aldazhanov, B. H. Hager, M. W. Hamburger, T. A. Herring, K. B. Kalabaev, V. I. Makarov, P. Molnar, S. V. Panasyuk, M. T. Prilepin, R. E. Rellinger, I. S. Sadybakasov, B. J. Souter, Yu. A. Trapeznikov, V. Ye. Tsurkov, and A. V. Zubovich (1996). Relatively resent construction of the Tien Shan inferred from GPS measurements of present-day crustal deformation rates, *Nature* **384,** 450–453.

Babuska, V., and J. Plomerova (2001). Subcrustal lithosphere around the Saxothuringian–Moldanubian Suture Zone: a model derived from anisotropy of seismic wave velocities, *Tectonophysics* **332,** 185–199.

Babuska, V., J. Plomerova, and J. Sileny (1993). Models of seismic anisotropy in the deep continental lithosphere, *Phys. Earth Planet. Interiors* **78,** 167–191.

Backus, G. E. (1965). Possible forms of seismic anisotropy of the uppermost mantle under oceans, *J. Geophys. Res.* **70,** 3429–3439.

Backus, G. E. (1970). A geometrical picture of anisotropic elastic tensors, *Rev. Geophys. Space. Phys.* **8,** 633–671.

Belousov, N. V., N. I. Pavlenkova, and G. N. Kvyatkovskaya (1992). Structure of the crust and upper mantle of the [former] USSR, *Int. Geol. Rev.* **98,** 6755–6804.

Bijwaard, H., W. Spakman, and E. R. Engdahl (1998). Closing the gap between regional and global travel time tomography, *J. Geophys. Res.* **103,** 30,055–30,078.

Bokelmann, G. H. R. (2002). Convection-driven motion of the North American craton: evidence from *P*-wave anisotropy, *Geophys. J. Int.* **148,** 278–287.

Bormann, P., P.-T. Burghardt, L. I. Makeyeva, and L. P. Vinnik (1993). Teleseismic shear-wave splitting and deformations in central Europe, *Phys. Earth Planet. Interiors* **78,** 157–166.

Bump, H. A., and A. F. Sheehan (1998). Crustal thickness variations across the northern Tien Shan from teleseismic receiver functions, *J. Geophys. Res.* **25,** 1055–1058.

Crampin, S., and D. Bamford (1977). Inversion of *P*-wave velocity anisotropy, *Geophys. J. R. Astr. Soc.* **49,** 123–132.

Dziewonski, A. M., and D. L. Anderson (1983). Travel times and station corrections for *P* waves at teleseismic distances, *J. Geophys. Res.* **88,** 3295–3314.

Friederich, W. (2004). The *S*-velocity structure of the East Asian mantle from inversion of shear and surface waveforms, *Geophys. J. Int.* (in press).

Ghose, S., M. W. Hamburger, and J. Virieux (1998). Three-dimensional velocity structure and earthquake locations beneath the northern Tien Shan of Kyrgyzstan, central Asia, *J. Geophys. Res.* **103,** 2725–2748.

Goldstein P., W. R. Walter, and G. Zandt (1992). Upper mantle structure beneath central Eurasia using a source array of nuclear explosions and waveforms at regional distances, *J. Geophys. Res.* **97,** 14,097–14,113.

Griffiths, R. W., and I. H. Campbell (1990). Stirring and structure in mantle starting plumes, *Earth Planet. Sci. Lett.* **99,** 66–78.

Hager, B. H., R. W. King, and M. H. Murray (1991). Measurement of crustal deformation using the Global Positioning System, *Ann. Rev. Earth Planet. Sci.* **19,** 351–382.

Helffrich, G., P. Silver, and H. Given (1994). Shear-wave splitting variation over short spatial scales on continents, *Geophys. J. Int.* **119,** 561–573.

Herrin, E., and J. Taggart (1968). Regional variation in *P* travel times, *Bull. Seism. Soc. Am.* **58,** 1325–1337.

Junga, S. L. (1990). *Methods and Results of Investigation of Seismotectonic Deformations*, Nauka, Moscow, 191 pp. (in Russian).

Karki, B. B., L. Stixrude, S. J. Clark, M. C. Warren, G. J. Ackland, and J. Crain (1997). Structure and elasticity of MgO at high pressure, *Am. Mineral.* **82,** 51–60.

Kendall, J. M., and P. G. Silver (1996). Constraints from seismic anisotropy on the nature of the lowermost mantle, *Nature* **381,** 409–412.

Kennett, B. L. N., and E. R. Engdahl (1991). Travel times for global earthquake location and phase identification, *Geophys. J. Int.* **105,** 429–465.

Kondorskaya, N. V., and N. V. Shebalin (1982). New Catalog of Strong Earthquakes in the U.S.S.R. from Ancient Times through 1977, Report SE31, World Data Center for Solid Earth Geophysics, Boulder, Colorado, 608 pp.

Levin, V., and J. Park (1997). *P-SH* conversions in a flat-layered medium with anisotropy of arbitrary orientation, *Geophys. J. Int.* **131,** 253–266.

Liu, K., Z. J. Zhang, J. F. Hu, and J. W. Teng (2001). Frequency band-dependence of *S*-wave splitting in China mainland and its implications, *Sci. China D Earth Sciences* **44,** 659–665.

Mahdi, H., and G. L. Pavlis (1998). Velocity variations in the crust and upper mantle beneath the Tien Shan inferred from Rayleigh wave dispersion: implications for tectonic and dynamic process, *J. Geophys. Res.* **103,** 2693–2703.

Makeyeva, L. I., L. P. Vinnik, and S. W. Roecker (1992). Shear-wave splitting and small-scale convection in the continental upper mantle, *Nature* **358,** 144–147.

Marson-Pidgeon, K., and M. K. Savage (1997). Frequency-dependent anisotropy in Wellington, New Zealand, *Geophys. Res. Lett.* **24,** 3297–3300.

Martynov, V. G., F. L. Vernon, R. J. Mellors, and G. L. Pavlis (1999). High-frequency attenuation in the crust and upper mantle of the northern Tien Shan, *Bull. Seism. Soc. Am.* **89,** 215–238.

McNamara, A. K., P. E. van Keken, and S.-I. Karato (2002). Development of anisotropic structure in the Earth's lower mantle by solid-state convection, *Nature* **416,** 310–314.

Mellors, R. J., F. L. Vernon, G. L. Pavlis, G. A. Abers, M. W. Hamburger, S. Ghose, and B. Iliasov (1997). The M_S = 7.3 1992 Suusamyr, Kyrgyzstan, earthquake, part I: Constraints on fault geometry and source parameters based on aftershocks and body-wave modeling, *Bull. Seism. Soc. Am.* **87,** 11–22.

Minster, J. B., and T. H. Jordan (1978). Present-day plate motions, *J. Geophys. Res.* **83,** 5331–5354.

Montagner, J.-P., and B. L. N. Kennett (1996). How to reconcile body-wave and normal-mode reference Earth models, *Geophys. J. Int.* **125,** 229–248.

Morgan, W. J. (1971). Convection plumes in the lower mantle, *Nature* **230,** 42–43.

Morris, G. B., R. W. Raitt, and G. G. Shor, Jr. (1969). Velocity anisotropy and delay-time maps of the mantle near Hawaii, *J. Geophys. Res.* **74,** 4300–4316.

Muirhead, K. (1985). Comments on "Reflection properties of phase transition and compositional change models of the 670-km discontinuity" by A. C. Lees, S. T. Bukowinsky, and R. Jeanloz, *J. Geophys. Res.* **90,** 2057–2059.

Olson, P. (1987). Drifting mantle hotspots, *Nature* **327,** 559–560.

Oreshin, S., L. Vinnik, D. Peregudov, and S. Roecker (2002). Lithosphere and astenosphere of the Tien Shan imaged by *S* receiver functions, *Geophys. Res. Lett.* **8,** 1191.

Plomerova, J., R. Arvidsson, V. Babuska, M. Granet, O. Kulhanek, G. Poupinet, and J. Sileny (2001). An array study of lithospheric structure across the Protogine zone, Varmland, south-central Sweden: signs of a paleocontinental collision, *Tectonophysics* **332,** 1–21.

Press, W. H., B. P. Flannery, S. A. Teukolsky, and W. T. Vetterling (1986). *Numerical Recipes*, Cambridge U Press, New York, 818 pp.

Roecker, S. W., T. M. Sabitova, L. P. Vinnik, Yu. A. Burmakov, M. I. Golvanov, R. Mamatkanova, and L. Munirova (1993). Three-dimensional elastic wave velocity structure of the western and central Tien Shan, *J. Geophys. Res.* **98,** 15,779–15,795.

Sabitova, T. M. (1978). Structure of the Earth's crust of northern Kyrgyzstan and bordered region of the southeastern Kazakhstan from seismological data, in *Structure of the Earth's Crust and the Seismicity of the Northern Tien Shan*, Ilim, Frunze, Kyrgyzstan, 4–21 (in Russian).

Sabitova, T. M. (1986). Structure of the Earth's crust from seismological data, in *Lithosphere of the Tien Shan*, Nauka, Moscow, 56–63 (in Russian).

Sabitova, T. M. (1989). *Structure of the Earth's Crust of the Kyrgyz Tien Shan from the Seismological Data*, Ilim, Frunze, Kyrgyzstan, 173 pp. (in Russian).

Sadybakasov, I. (1990). *Neotectonics of High Asia*, Nauka, Moscow, 176 pp. (in Russian).

Savage, M. K. (1999). Seismic anisotropy and mantle deformation: what have we learned from shear wave splitting? *Rev. Geophys.* **37,** 65–106.

Savage, M., and P. G. Silver (1993). Mantle deformation and tectonics: constraints from seismic anisotropy in the western United States, *Phys. Earth Planet. Interiors* **78,** 207–228.

Shen, Y., S. C. Solomon, I. T. Bjarnason, G. Nolet, W. J. Morgan, R. M. Allen, K. Vogfjord, S. Jakobsdottir, R. Stefansson, B. R. Julian, and G. R. Foulger (2002). Seismic evidence for a tilted mantle plume and north–south mantle flow beneath Iceland, *Earth Planet. Sci. Lett.* **197,** 261–272.

Silver, P. G. (1996). Seismic anisotropy beneath the continents: probing the depths of geology, *Ann. Rev. Earth Planet. Sci.* **24,** 385–432.

Silver, P. G., and W. W. Chan (1991). Shear wave splitting and subcontinental mantle deformation, *J. Geophys. Res.* **96,** 16,429–16,454.

Silver, P. G., R. P. Meyer, D. E. James, and S. B. Shirey (1989). A portable experiment to determine properties of the subcontinental mantle: preliminary results, *EOS* **70,** 1227.

Steinberger, B. (2000). Plumes in a convecting mantle: models and observations for individual hotspots, *J. Geophys. Res.* **105,** 11,127–11,152.

Steinberger, B., and R. J. O'Conell (1998). Advection of plumes in mantle flow: implications for hotspot motion, mantle viscosity, and plume distribution, *Geophys. J. Int.* **132,** 412–434.

Tapponnier, P., and P. Molnar (1979). Active faulting and Genozoic tectonics of the Tien Shan, Mongolia, and Baykal regions, *J. Geophys. Res.* **84,** 3425–3459.

Van der Hilst, R. D., S. Widiyantoro, and E. R. Engdahl (1997). Evidence for deep mantle circulation from global tomography, *Nature* **386,** 578–584.

Vernon, F. (1992). Kyrghizstan seismic telemetry network, *IRIS Newsl.* **11,** 7–9.

Vetter, U., and J.-B. Minster (1981). P_n velocity anisotropy in southern California, *Bull. Seism. Soc. Am.* **71,** 1511–1530.

Vinnik, L. P. (1989). Mantle discontinuities, in *The Encyclopedia of Solid Earth Geophysics*, D. E. James (Editor), Van Nostrand Reinhold, New York, 802–806.

Vinnik, L. P., and J.-P. Montagner (1996). Shear wave splitting in the mantle *Ps* phase, *Geophys. Res. Lett.* **23,** 2449–2452.

Vinnik, L. P., and A. M. Saipbekova (1984). Structure of the lithosphere and the asthenosphere of the Tien Shan, *Ann. Geophys.* **2,** 621–626.

Vinnik, L. P., S. Chevrot, and J.-P. Montagner (1998). Seismic evidence of flow at the base of the upper mantle, *Geophys. Res. Lett.* **25,** 1995–1998.

Vinnik, L., D. Peregudov, L. Makeyeva, and S. Oreshin (2002a). Towards 3-D fabric in the continental lithosphere and asthenosphere: the Tien Shan, *Geophys. Res. Lett.* **16,** 1791.

Vinnik, L. P., S. Roecker, G. L. Kosarev, S. I. Oreshin, and I. Yu. Koulakov (2002b). Crustal structure and dynamics of the Tien Shan, *Geophys. Res. Lett.* **22,** 2047.

Whitehead, J. A. (1982). Instabilities of fluid conduits in a flowing Earth: are plates lubricated by the asthenosphere? *Geophys. J. R. Astr. Soc.* **70,** 415–433.

Wolfe, C. J., and F. L. Vernon, III (1998). Shear-wave splitting at central Tien Shan: evidence for rapid variation of anisotropic patterns, *Geophys. Res. Lett.* **25,** 1217–1220.

Wookey, J., J. M. Kendall, and G. Barruol (2002). Mid-mantle deformation inferred from seismic anisotropy, *Nature* **415,** 777–780.

Yamazaki, D., and S. Karato (2004). Fabric development in (Mg,Fe)O during large strain, shear deformation: implications for seismic anisotropy in Earth's lower mantle, *Phys. Earth Planet. Interiors* (in press).

Zhao, D. (2001). Seismic structure and origin of hotspots and mantle plumes, *Earth Planet. Sci. Lett.* **192,** 251–265.

Zonenshain, L. P., M. I. Kuzmin, and L. M. Natapov (1990). *Geology of the USSR: A Plate Tectonic Synthesis*, American Geophysical Union Geodynamics Ser. **21,** Washington, D.C.

Zubovich, A. V., Yu. A. Trapeznikov, V. D. Bragin, O. I. Mosienko, G. G. Shelochkov, A. K. Rybin, and Y. Yu. Batalev (2001). Deformation field, Earth's crust deep structure, and spatial seismicity distribution in the Tien Shan, *Geol. Geophys.* **42,** 1634–1640 (in Russian).

Institute of Geophysics and Planetary Physics (0225)
Scripps Institution of Oceanography
La Jolla, California 92093
(V.G.M., F.L.V., D.L.K.)

Rensselaer Polytechnic Institute
Department of Geology
Troy, New York 12180-3590
(S.W.R.)

Manuscript received 16 January 2003.